

## Article

# Refill Friction Stir Spot Welding of an Al-Li Alloy: The Effects of Rotating Speed and Welding Time on Joint Microstructure and Mechanical Properties

Yuanbiao Cui <sup>1</sup>, Binbin Wang <sup>1</sup>, Wenzhe Dong <sup>1</sup>, Zhengwei Li <sup>2,\*</sup>  and Jiuchun Yan <sup>2</sup>

<sup>1</sup> School of Mechatronics Engineering, Harbin Vocational & Technical College, Harbin 150081, China; 15004698066@163.com (Y.C.); 15104511740@163.com (B.W.); dongwenzhe1988@126.com (W.D.)

<sup>2</sup> State Key Laboratory of Precision Welding & Joining of Materials and Structures, Harbin Institute of Technology, Harbin 150001, China; jcyan@hit.edu.cn

\* Correspondence: lizhengwei@hit.edu.cn

**Abstract:** In this work, 2060 Al-Li alloy was joined by refill friction stir spot welding (RFSSW). The effects of the tool's rotating speed and welding time on the microstructure and mechanical properties of the welded joints were studied. The results showed that joints without defects can be obtained within a wide range of welding parameters. Tiny voids were formed when using a low rotating speed of 1600 rpm, and incomplete refilling was obtained when using a short welding time of 1 s. Increasing the rotating speed from 1600 to 2000 rpm increased the grain size of the stir zone (SZ). When using a short welding time of 1 s, the grains of the SZ were not completely broken with high orientation differences in the grains. Higher hardness was obtained in the SZ when using a lower rotating speed and shorter welding time. Increasing the rotating speed increased the joint strength, while short and long welding times decreased the joint strength.

**Keywords:** refill friction stir spot welding; 2060 Al-Li alloy; tool rotating speed; welding time; grain size; hardness



**Citation:** Cui, Y.; Wang, B.; Dong, W.; Li, Z.; Yan, J. Refill Friction Stir Spot Welding of an Al-Li Alloy: The Effects of Rotating Speed and Welding Time on Joint Microstructure and Mechanical Properties. *Metals* **2024**, *14*, 1383. <https://doi.org/10.3390/met14121383>

Academic Editor: Masahiro Fukumoto

Received: 28 October 2024  
Revised: 27 November 2024  
Accepted: 30 November 2024  
Published: 2 December 2024



**Copyright:** © 2024 by the authors. Licensee MDPI, Basel, Switzerland. This article is an open access article distributed under the terms and conditions of the Creative Commons Attribution (CC BY) license (<https://creativecommons.org/licenses/by/4.0/>).

## 1. Introduction

Al alloys have advantages of low densities, high specific strengths, low costs, and good corrosion resistance. Al alloys serve as an indispensable key structural material in the global aerospace field [1,2]. In modern aviation industry, Al alloy is one of the most important materials in an aircraft's body structure, and it can save about 40% to 70% the weight of the body structure. Al alloys are widely used in the main bearing frame, beam, wall panel, skin, and other parts of an aircraft [3]. After nearly 100 years of development, aviation Al alloy has become a core key supporting material for aerospace. Al-Li alloy refers to a class of Al alloys with Li element as one of their main alloying elements. Li element is the least dense metal element with a density of only 0.534 g/cm<sup>3</sup>. Li element can reduce the density of Al alloy, improve its elastic modulus, and increase its strength. Al-Li alloy has the advantages of a high specific strength and a high specific modulus, and it has become a key material to achieve structural lightweight property [4,5].

The further applications of Al-Li alloys inevitably involve their joining with themselves or other alloys. However, Al alloys can melt during fusion welding processes, easily causing defects such as pores, large distortions, high residual stresses, and hot cracks [6,7]. These defects seriously limit further applications of Al alloys. Fortunately, such problems can be solved by solid-state joining methods. As a new solid-state joining technology, friction stir welding (FSW) is very suitable to join Al alloys [8–10]. When joining Al alloys by FSW, the peak joining temperature is below their melting points [11], and thus, some of the above-mentioned melting defects can be avoided. Since the invention of FSW, it has been widely used to join different kinds of Al alloys and many important conclusions have

been drawn [12–14]. Tiwari et al. [12] joined AA2024 and AA7075 and studied the effect of different stress ratios on crack growth in the joints. They reported that the highest fatigue life of 45,000 cycles was observed at  $R = -0.5$ , while the lowest of 26,000 cycles was noted at  $R = 0.8$ . Fan et al. [13] used double-sided friction stir spot welding to join 2198-T8 Al alloy and reported a 47% increase in joint strength compared to the single-sided welding process. Tang et al. [14] used a synergistically double-sided friction stir welding (SDS-FSW) to join 6061 Al alloy and found that the joint strength is comparable to the base material when using 1400 rpm and 600 mm/min.

However, a keyhole is always left in the joint center after FSW [15,16], which significantly deteriorates the joint strength. To eliminate the keyhole, several methods have been attempted by researchers [17,18]. In 2003, the refill friction stir spot welding (RFSSW) method was invented by the GKSS [19]. RFSSW uses a complicated tool that consists of a clamping ring, a sleeve, and a pin [20,21]. These three components can move separately. The keyhole can be eliminated after applying specific movements on these three components [22]. In the last several decades, RFSSW has attracted wide attention and has been used to join various kinds of Al alloys [23–28].

So far, few works have used RFSSW to join Al-Li alloy and few valuable conclusions have been obtained. Therefore, in this work, RFSSW was used to join an Al-Li alloy. By using various tool rotating speeds and welding times, the microstructure and mechanical properties of the obtained joints were studied. The grain size, microstructure, and texture evolution in the joints were examined. Then, the mechanical properties of the joints, such as the hardness and the failure load, were studied. This work provides insights into joining Al-Li alloys and can promote its wide applications.

## 2. Experiments

The base metal (BM) is 2060 Al-Li alloy, provided by Northeast light alloy Co. Ltd. The chemical composition of 2060 alloy is shown in Table 1. The BM has a tensile strength of 520 MPa. The BM has a dimension of 140 mm × 40 mm × 2 mm (Figure 1e). The BM was polished with 500# sandpapers before welding. Lap joint configuration was used in this work. The lap width was 40 mm. An RFSSW machine named RPS100SK10, produced by Beijing FSW Technology Co., Ltd., was used during welding. The RFSSW tool consisted of three parts: a sleeve, a pin, and a clamping ring. The sleeve and pin were threaded to enhance the material flow behavior (Figure 1e). Three tool rotating speeds of 1600 rpm, 1800 rpm, and 2000 rpm were used. The plunging depth of 2.2 mm was used. Different welding times of 1 s, 2 s, and 4 s were used. The welding process is shown in Figure 1.

**Table 1.** Chemical composition of 2060 Al-Li alloy (weight %).

Alloy	Cu	Li	Fe	Mn	Mg	Zn	Si	Ag	Al
2060	3.56	0.72	0.026	0.3	0.72	0.34	0.025	0.086	Bal.

After welding, the joints were cut through their centers to fabricate metallographic samples. The cross sections of the joints were observed after polishing and etching. The grains at different regions of the joint were studied on a Zeiss scanning electron microscope (SEM, Carl Zeiss AG) equipped with electron back-scattered diffraction (EBSD) detectors. The hardness was tested on an HVS-1000 (Beijing Time High Technology Ltd.) machine. The testing force was 200 g, and the holding time was 10 s. Lap shear failure loads of the joints were tested on an AG-X Plus 250 kN/50 kN electronic universal tensile test machine (Shimadzu Corporation, Japan) using a speed of 3 mm/min. No less than three samples were tested for each parameter.

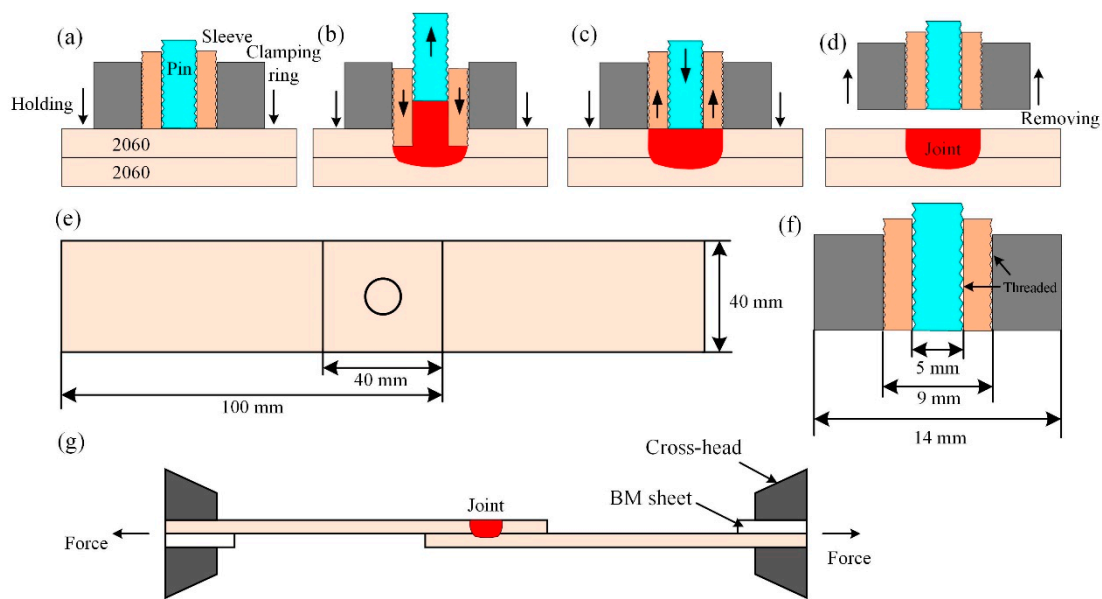
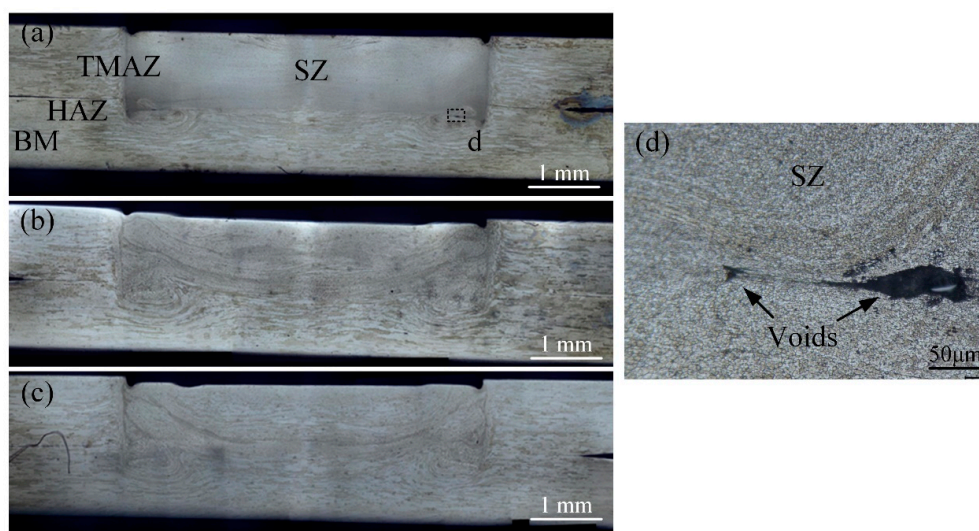


**Figure 1.** Joint configuration and welding process: (a) preheating, (b) sleeve plunging, (c) sleeve retracting, (d) tool removing, (e) joint configuration, (f) tool, and (g) schematic of tensile test.

### 3. Results and Discussions

#### 3.1. Cross-Sections of the Joints

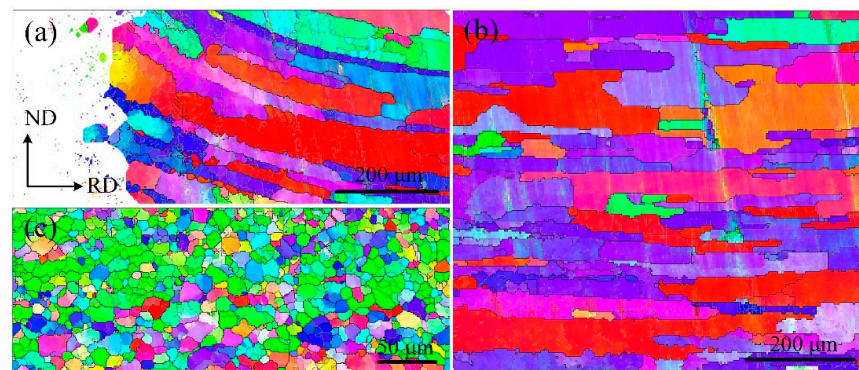
Figure 2 shows the cross-sections of the joints using different rotating speeds. Figure 2a shows the joint cross-section using 1600 rpm. The Al-Li alloys of the upper and lower sheets mix well with each other after undergoing the stirring action of the tool. No obvious variation is observed on the three joints when increasing the rotating speed. A tiny void with a size of approximately 50  $\mu\text{m}$  is obtained when using low rotating speed of 1600 rpm, as shown in Figure 2d. The void can be attributed to an insufficient-material-flow behavior. Similar to the traditional FSW joint, the joint can be divided into a stir zone (SZ), heat-affected zone (HAZ), thermo-mechanically affected zone (TMAZ), and BM, as shown in Figure 2a. The grains inside these different regions show different morphologies, sizes, and orientations, which are subsequently discussed.



**Figure 2.** Cross-section of the joint using (a) 1600 rpm, (b) 1800 rpm, and (c) 2000 rpm; (d) voids in the joint using 1600 rpm. The joint can be divided into a stir zone (SZ), heat-affected zone (HAZ), thermo-mechanically affected zone (TMAZ), and base material (BM).

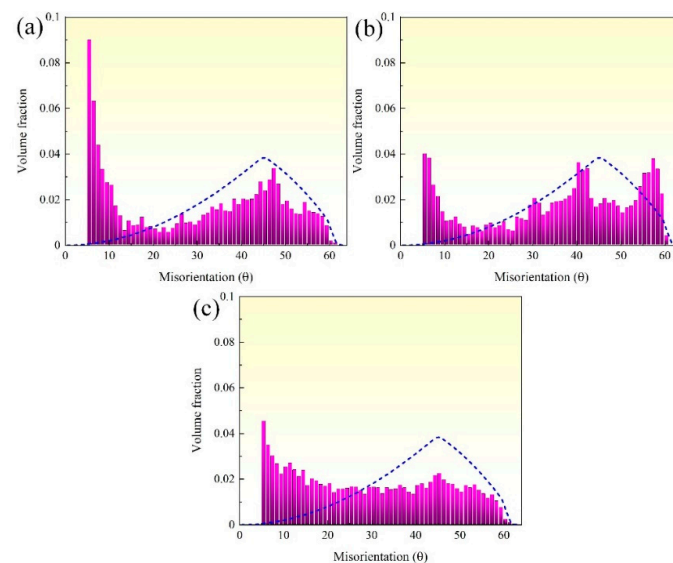
### 3.2. Microstructure at Different Regions of the Joint

Figure 3 shows the microstructure at different regions of the joint. The joint was joined using a rotating speed of 1600 rpm. Figure 3a shows the inverse pole figure (IPF) of the TMAZ and HAZ. The grains show bending morphologies in the TMAZ, which are formed due to the plunging of the tool. The grains near the SZ in the left region of the image have small sizes because they are broken by the tool stirring. The grains of the HAZ show obvious changes compared with the TMAZ. Figure 3b shows the IPF image of the grains at the BM. The grains are long and large because the sheet is rolled. Some grains have sizes larger than 200  $\mu\text{m}$ . Figure 3c shows the IPF of the grains in the SZ. Due to the intense mechanical stirring action caused by the tool, the grains in the SZ have very small sizes. The EBSD result shows that the grains have an average size of 9.67  $\mu\text{m}$ .



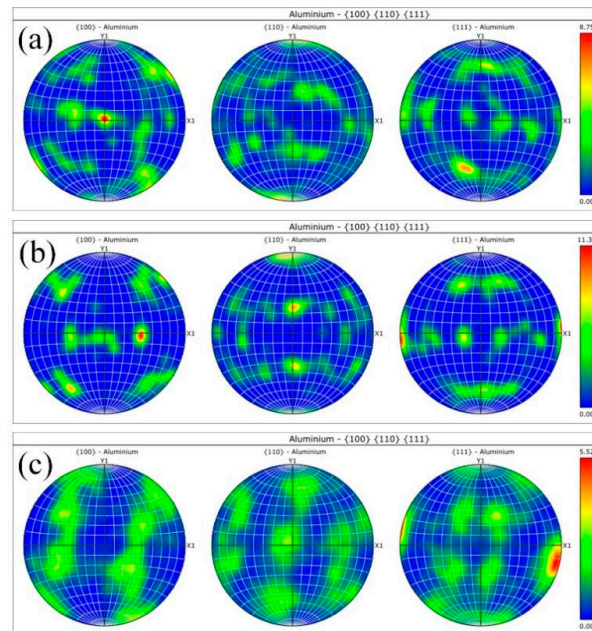
**Figure 3.** IPF image of (a) TMAZ and HAZ, (b) BM, and (c) SZ.

Figure 4 shows the misorientation distributions in different regions of the joint. Figure 4a shows the misorientation distribution in the TMAZ. Numerous low-angle boundaries (LABs) are observed, and they make up about 33.0%. Such a high value can be attributed to the inadequate breakage of the grains caused by the inadequate mechanical stirring action. Figure 4b shows the misorientation distribution of the BM. By contrast, the high angle boundaries (HABs) have a much higher ratio of 81.9% than the TMAZ (67.0%). Figure 4c shows the misorientation distribution in the SZ, which has a LABs ratio of 27.9%. This can be attributed to the fact that the SZ undergoes a more intense mechanical stirring action exerted by the rotating tool compared with the TMAZ.



**Figure 4.** Misorientation distribution in the (a) TMAZ, (b) BM, and (c) SZ.

Figure 5 shows the pole figures (PFs) at different regions of the joint. Figure 5a shows the PF of the TMAZ and HAZ. The result shows that the grains here have a preferred orientation of  $\langle 100 \rangle // \text{TD}$ . Figure 5b shows the PF of the BM, which shows preferred orientations of  $\langle 100 \rangle // \text{RD}$  and  $\langle 111 \rangle // \text{RD}$ . The PF of the SZ in Figure 5c shows that the SZ has a similar preferred orientation with the BM but has a lower multiple of uniform distribution (mud) value.

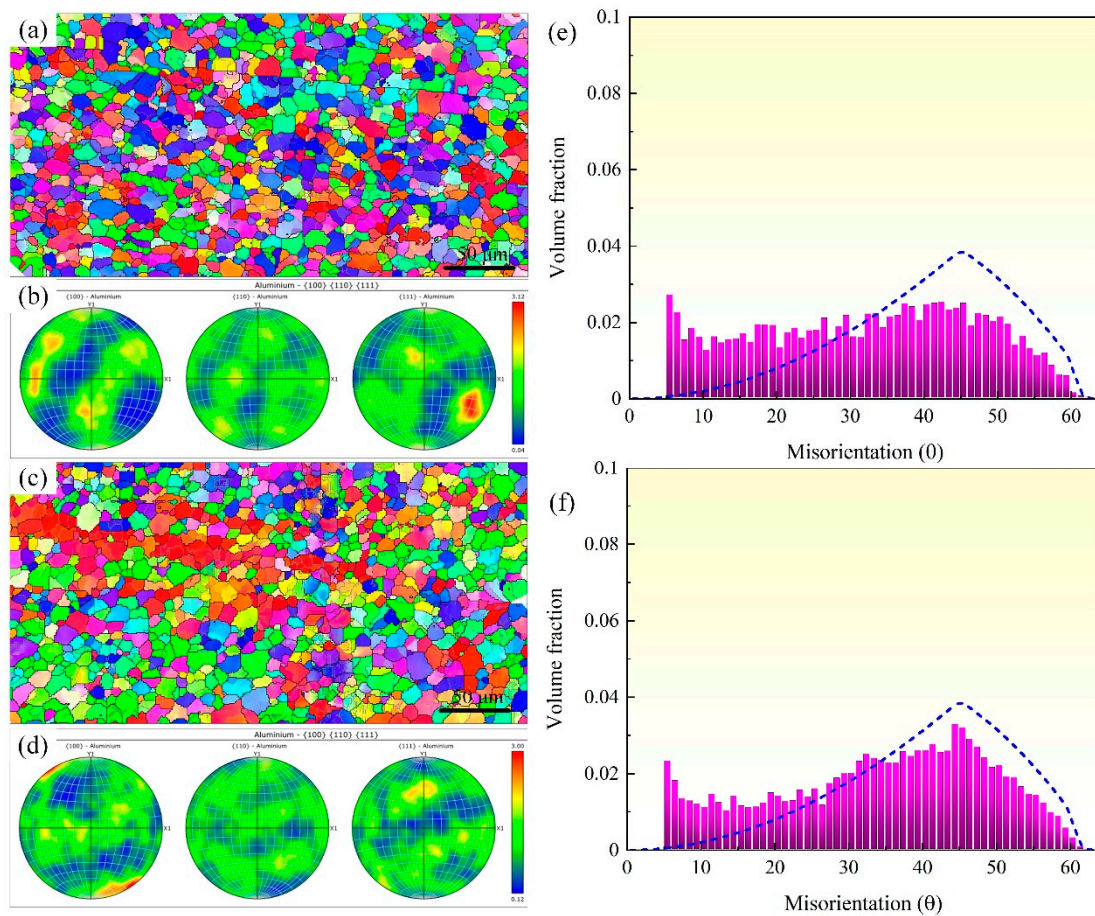


**Figure 5.** PF image of (a) TMAZ, (b) BM, and (c) SZ.

### 3.3. Effect of Rotating Speed on the Microstructure of the Joint

Figure 6 shows the microstructure of the joint using other welding parameters. Figure 6a shows the IPF of the joint's SZ using a rotating speed of 1800 rpm. Similar to the SZ taken from the joint using 1600 rpm, very fine grains are observed in the SZ. The EBSD result shows that the average grain size under such a condition is  $9.78 \mu\text{m}$ , which is slightly larger than those shown in Figure 3c. Such a result can be attributed to the fact that more heat input causes the grain's coarseness when using a higher rotating speed. A similar condition is obtained when using a higher rotating speed. Figure 6c shows the IPF of the SZ taken from the joint using a rotating speed of 2000 rpm. The EBSD result shows that the average grain size is  $10.75 \mu\text{m}$ , which is larger than those grains obtained using 1600 rpm and 1800 rpm.

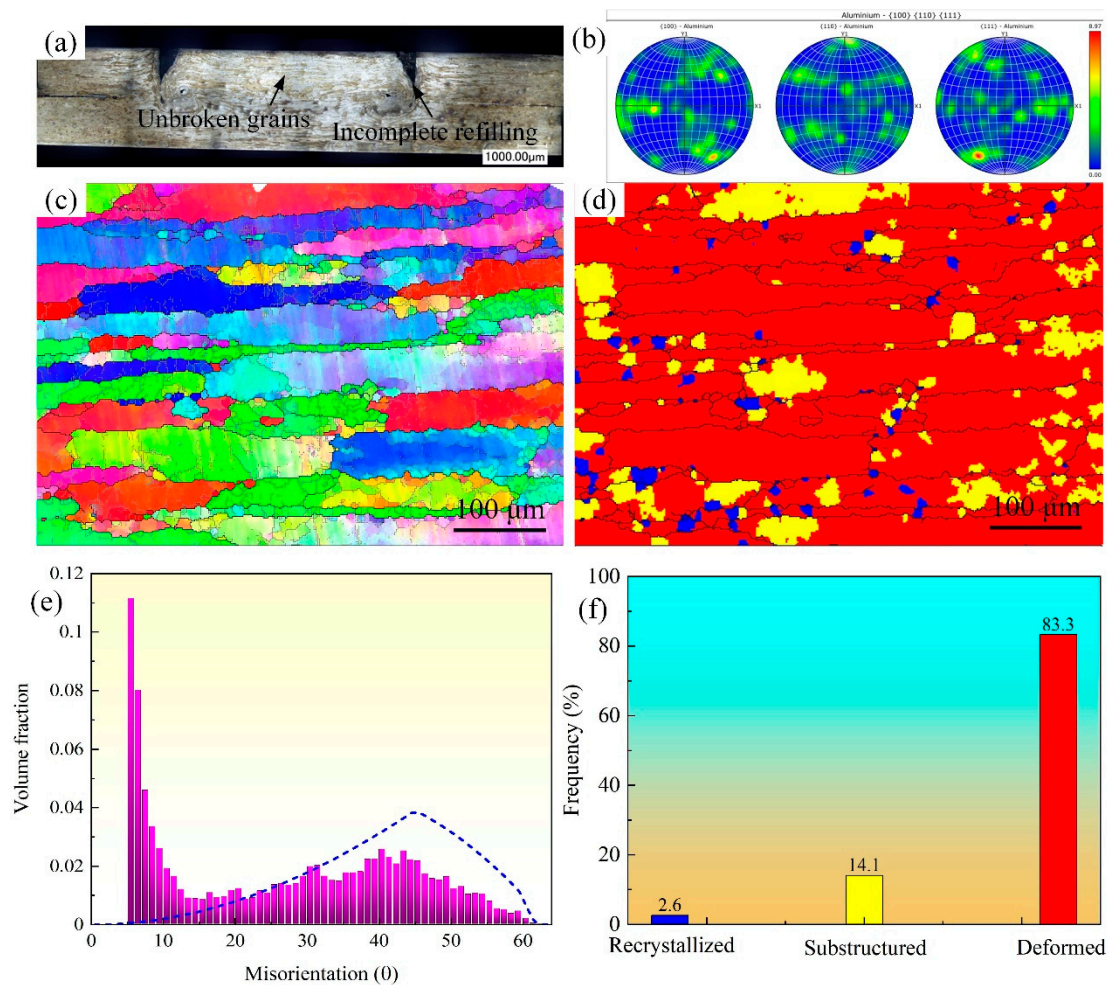
Figure 6b shows the PF of the grains using a rotating speed of 1800 rpm. The grains show no obvious texture under such a condition. The mud shows a low value of 3.12. A similar condition is obtained on the joint using 2000 rpm. As shown in Figure 6d, no obvious texture is observed, and the mud also has a low value of 3.0. Figure 6e shows the misorientation distributions using rotating speeds of 1800 rpm and 2000 rpm. The LABs have ratios of 20% and 30%, respectively. The lower value when using a rotating speed of 2000 rpm shown in Figure 6d shows that higher frictional heat can decrease the LABs.



**Figure 6.** Microstructure of the SZ: (a) IPF image of the SZ taken from the joint using 1800 rpm and its (b) PF and misorientation distribution (c); (d) IPF image of the SZ taken from the joint using 2000 rpm and its (e) PF and misorientation distribution (f).

### 3.4. Effect of Welding Time on the Microstructure of the Joint

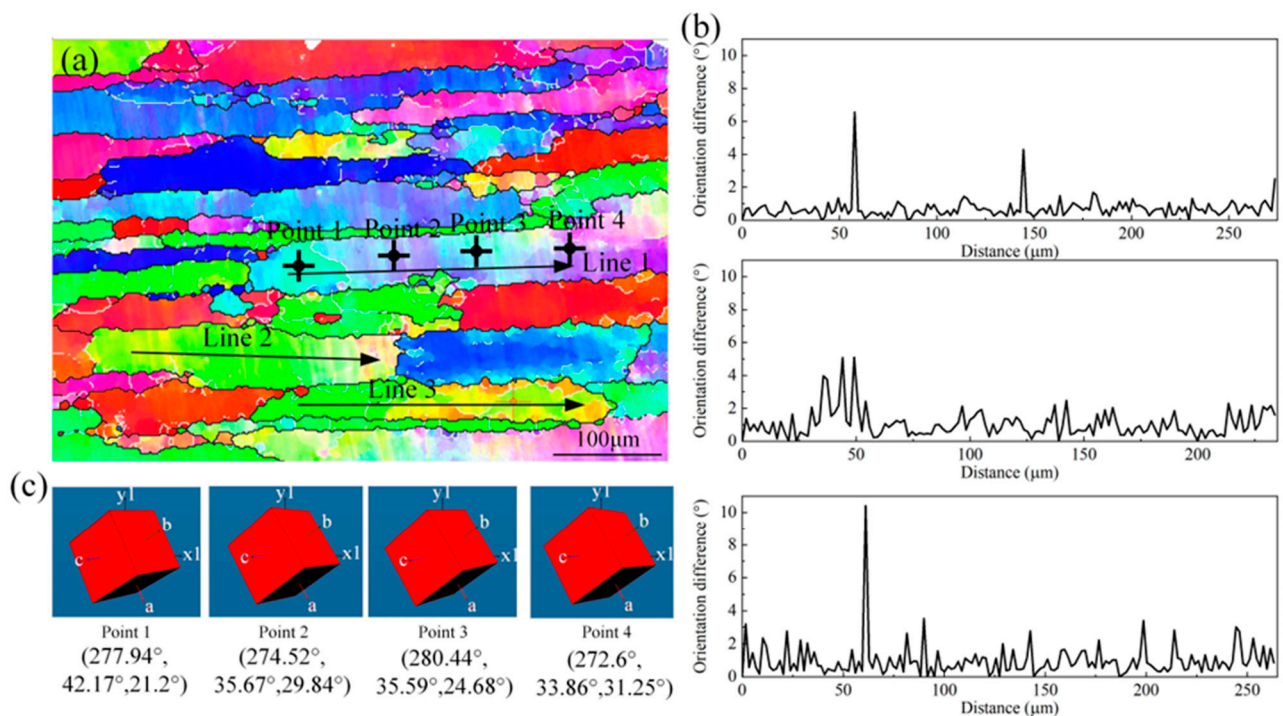
Figure 7 shows the microstructure of the joint using a short welding time of 1 s. Worth mentioning is that the cross-section morphology is taken after etching with Keller's reagent for 20 s (1% HF, 1.5% HCL, 2.5% HNO<sub>3</sub>, and 95% H<sub>2</sub>O). As shown in Figure 7a, a large incomplete refilling defect is observed on the two sides of the joint. This defect has a size larger than 1 mm. Also, voids with small sizes are observed at the maximum plunge depth region. This can be attributed to the incomplete material flow behavior caused by a short welding time. Such a result can also be proven by the microstructure in the SZ. Figure 7c shows the IPF image at the center of the joint. The result shows that very large grains are observed in this region. The material in this region is not completely broken by the stirring action of the tool. Figure 7b shows the PF of the grains in this region. The result shows that the grain in such a region has a high mud value of 8.97. Also, these grains have no obvious texture, only forming a weak preferred orientation of  $\langle 111 \rangle // \text{ND}$  with a rotation of 30°. The grain type distribution inside this region is shown in Figure 7d, and the result shows that most of the grains are deformed grains. Figure 7f shows that the deformed grains have a high ratio of 83.3%. The misorientation distribution inside this region is shown in Figure 7e. The result shows that this region has a very high LAB ratio of 89%, which is very close to that of the TMAZ. This is because the grains here undergo an incomplete mechanical stirring effect and are not completely broken. Therefore, numerous dislocations form in such a region and then form LABs.



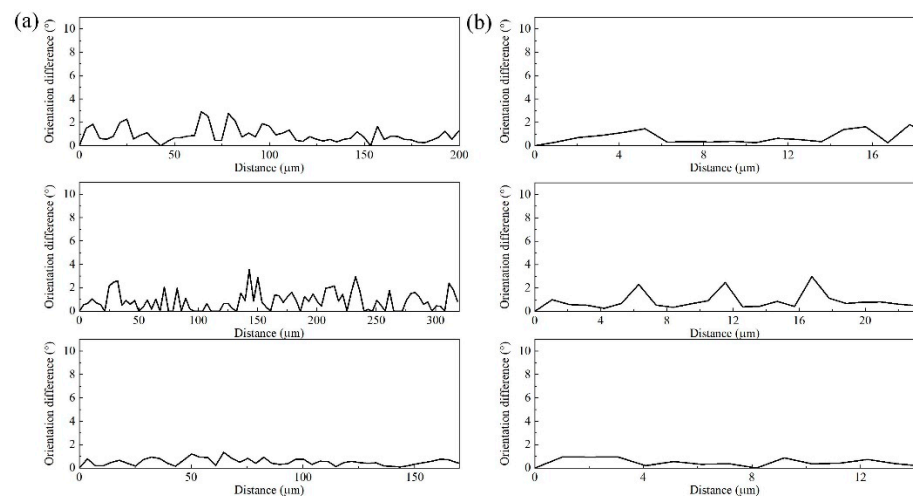
**Figure 7.** Microstructure of the joint using a short joining time of 1 s: (a) joint cross section, (b) PF image of the SZ, (c) IPF of the SZ, (d) grain type, (e) misorientation distribution, and (f) grain type ratio.

Figure 7c shows that when using a low welding time, not only some defects like incomplete refilling appear, but also the grains inside the SZ are not completely broken. Here, we tested the orientation difference inside the grains of the SZ. Figure 8a shows the testing positions. As shown in Figure 8a, although the grains are not completely broken, different orientations exist in different regions. The orientation variations inside different grains were tested, and the results are shown in Figure 8b. From Figure 8b, we can see that large orientation differences were obtained inside the long grains. A high difference of over  $10^\circ$  was even obtained. Moreover, the orientation at some specific points was also tested. As shown in Figure 8c, four different values were obtained inside one grain.

To illustrate the large orientation differences of the grain in the SZ using a short welding time, we also tested the orientation in other regions of the joint. Figure 9a shows the orientation difference inside the three grains of the BM. The results show that the orientation differences are very low inside the BM. The orientation differences inside the SZ are shown in Figure 9b. Similarly, quite low orientation differences were obtained, which can be attributed to the complete break and recrystallization of the grains in the SZ.



**Figure 8.** The large orientation difference inside the stir zone: (a) testing region, (b) orientation difference inside different grains, (c) orientation at different points.



**Figure 9.** Orientation within one grain of (a) BM and (b) SZ of the joint in Figure 2c.

### 3.5. Hardness of the Joints

Figure 10 shows the hardness of the joints using different welding parameters. Figure 10a shows the hardness of the joint using different rotating speeds. The result shows that the Al-Li alloy substrate has a hardness value of approximately 105 HV. The SZ formed using a rotating speed of 2000 rpm had an almost-equal hardness compared with the BM. Decreasing the rotating speed from 2000 rpm to 1600 rpm could decrease the grain size in the SZ, as shown in Figure 5. Thus, the hardness of the SZ shows a slight increase. As shown in Figure 10a, a high hardness value of approximately 120 HV was obtained when using a rotating speed of 1600 rpm. Figure 10b shows the hardness of the joint using different welding times. In general, the joint using a welding time of 4 s has the lowest hardness. This can be attributed to the higher heat input caused by the longer welding

time. The joint welded using a rotating speed of 1 s has a higher hardness value, which can be attributed to the lowest softness of the joint.

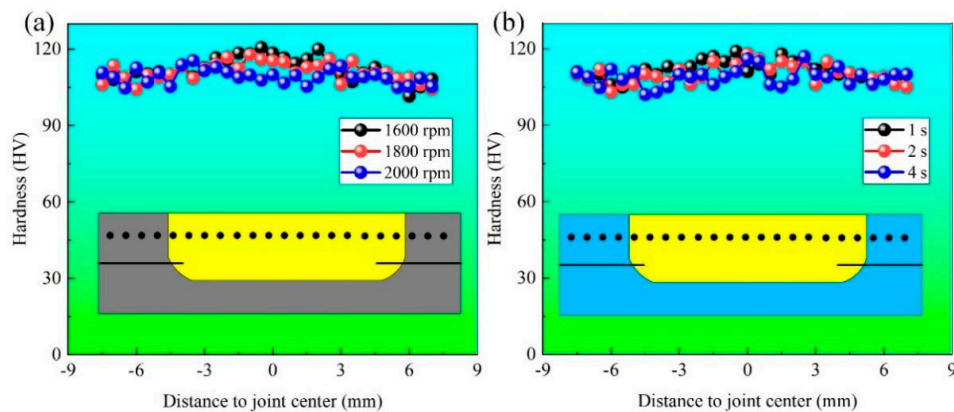


**Figure 10.** Hardness of the joints in the upper SZ using (a) different rotating speeds and (b) different welding times.

### 3.6. Tensile Properties of the Joints

Figure 11a shows the lap shear failure load of the joint. We can see that the tiny void formed in the joint bottom hardly affects the joint strength. This can be attributed to the fact that the failure crack (Figure 11b) does not propagate through the void. The joint strength still shows a slight increase with the increase in the rotating speed to 2000 rpm. This may be because the material mixing becomes better at higher rotating speeds. The grain size and the hardness have little influence on the joint strength. As shown in Figure 6a, large-defect of incomplete refilling is observed when using a welding time of 1 s. Under this condition, the joint has a low strength of 5.9 kN. The joint strength significantly increases and then becomes stable when using long welding times of 2 s and 4 s. Such a result shows that the welding time has a more significant effect on the joint strength than the rotating speed.

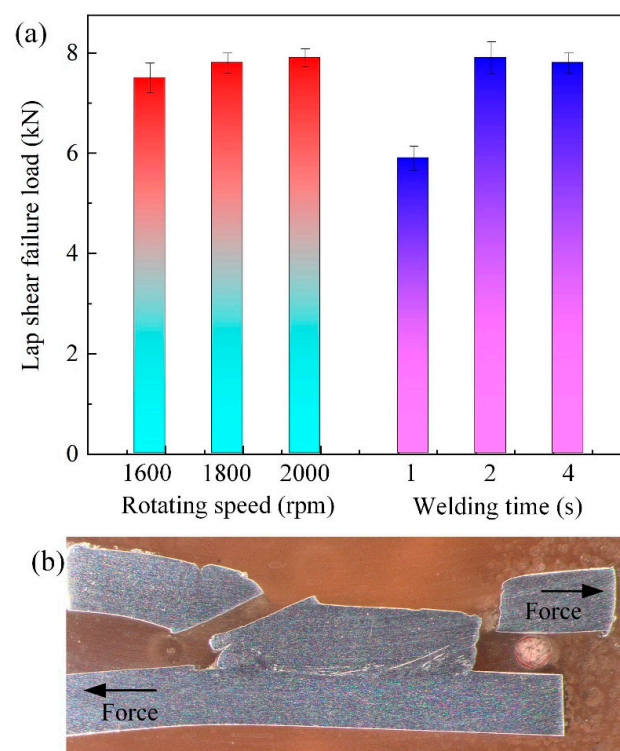


**Figure 11.** Tensile properties of the joints: (a) failure loads of the joints and (b) fracture position.

#### 4. Conclusions

In this work, the RFSSW method was used to join an Al-Li alloy. The effects of the tool's rotating speed and welding time on the microstructure of the joints were studied. The grains of the joints were studied by EBSD; the hardness and lap shear failure of the joint were also studied. The following conclusions can be drawn:

1. The joints show similar morphologies with changing rotating speed. A tiny void is obtained when using a low rotating speed of 1600 rpm.
2. Increasing the rotating speed causes the coarseness of the grains in the SZ due to the increased heat input. The grains in the SZ are not completely broken when using a short welding time of 1 s. Although not completely broken, the long grains in the SZ show different orientations in different regions inside one grain.
3. Both a low rotating speed and a short welding time cause an increase in the hardness of the joint. Increasing the rotating speed results in a slight increase in the failure load of the joint. The failure strength of the joint first increases and then decreases with an increase in the welding time. A maximum failure load of 7.9 kN is obtained when using a welding time of 2 s.

**Author Contributions:** Conceptualization, Z.L. and J.Y.; methodology, B.W. and W.D.; formal analysis, Z.L.; investigation, B.W. and W.D.; resources, Y.C. and Z.L.; data curation, Y.C., B.W., and W.D.; writing—original draft preparation, Z.L.; writing—review and editing, Z.L.; supervision, J.Y.; project administration, J.Y.; funding acquisition. All authors have read and agreed to the published version of the manuscript.

**Funding:** This project was supported by New Era Excellent Master's and Doctor's thesis of Heilongjiang Province (LJYXL2022-043) and the Natural Science Foundation of Chongqing (No. CSTB2023NSCQ-MSX0638).

**Data Availability Statement:** Data used to support the findings of this study are available from the corresponding author upon request.

**Conflicts of Interest:** The authors declare no conflicts of interest.

#### References

1. Wu, B.; Wang, Y.; Liu, X.; Zhang, D.; Zhou, S.; Deng, L.; Wang, L.; Li, H. Investigation on dynamic deformation behavior of 7A75 aluminum alloy over wide strain rates and constitutive model establishment. *J. Mater. Res. Technol.* **2024**, *30*, 5963–5976. [[CrossRef](#)]
2. Lipińska, M.; Pixner, F.; Szachogłuchowicz, I.; Mittermayr, F.; Grengg, C.; Enzinger, N.; Lewandowska, M. Application of electron beam welding technique for joining coarse-grained and ultrafine-grained plates from Al-Mg-Si alloy. *J. Manufact. Process.* **2023**, *104*, 28–43. [[CrossRef](#)]
3. Casalegno, V.; Smeacetto, F.; Salvo, M.; Sangermano, M.; Bains, F.; Noé, C.; Orlandi, M.; Piavani, R.; Bonfanti, R.; Ferraris, M. Study on the joining of ceramic matrix composites to an Al alloy for advanced brake systems. *Ceram. Int.* **2021**, *47*, 23463–23473. [[CrossRef](#)]
4. Chen, D.; Zhan, X.; Liu, T.; Zhao, Y.; Qi, N.; Sun, L. Effect of porosity morphology and elements characteristics on mechanical property in T-joints during dual laser-beam bilateral synchronous welding of 2060/2099 Al-Li alloys. *Opt. Laser. Technol.* **2021**, *140*, 107019. [[CrossRef](#)]
5. Zhou, X.; Zhao, H.; Liu, F.; Yang, B.; Xu, B.; Chen, B.; Tan, C. Effects of beam oscillation modes on microstructure and mechanical properties of laser welded 2060 Al-Li alloy joints. *Opt. Laser. Technol.* **2021**, *144*, 107389. [[CrossRef](#)]
6. Li, Q.; You, G.; Ling, X.; Zhou, P.; Wang, L.; Feng, J.; Zeng, S.; Tong, X.; Jiang, B. Enhancing fusion welding in die-cast Mg alloys: A combined ultrasonic vibration and hot rolling approach for porosity reduction, microstructure refinement, and mechanical property improvement. *J. Mater. Process. Technol.* **2024**, *331*, 118513. [[CrossRef](#)]
7. Lee, J.; Jang, J.; Lee, S.; Kang, M.; Lim, T.; Lee, S.H. Mitigating solidification cracking during the laser welding of extruded Al-Mg-Si alloys by tailoring the microstructure. *Eng. Sci. Technol.* **2024**, *55*, 101759. [[CrossRef](#)]
8. Xu, Z.; Li, Z.; Ji, S.; Zhang, L. Refill friction stir spot welding of 5083-O aluminum alloy. *J. Mater. Sci. Technol.* **2018**, *34*, 878–885. [[CrossRef](#)]
9. Song, Q.; Han, Z.; Hu, Y.; Wang, D.; Ren, Z.; Zhou, J.; Zhang, Z.; Zhao, H. Investigations on mechanical and surface properties of friction stir welded dissimilar joints of 2507 SDSS and 317L ASS. *Tribol. Int.* **2024**, *201*, 110226. [[CrossRef](#)]

10. Xue, W.; Song, N.; Li, J.; Huang, C.; He, D.; Ren, X. Improving mechanical properties of 18 mm thick plate friction stir welding joint by combining the thermomechanical-fluid coupled model and partial least squares regression algorithm. *J. Manuf. Process.* **2024**, *126*, 443–470. [[CrossRef](#)]
11. Anandan, B.; Manikandan, M. Machine learning approach for predicting the peak temperature of dissimilar AA7050-AA2014A friction stir welding butt joint using various regression models. *Mater. Lett.* **2022**, *325*, 132879. [[CrossRef](#)]
12. Tiwari, S.; Verma, S.; Kaushik, P. Investigating the influence of stress ratio variation on the crack growth rate in friction stir welded dissimilar aluminum alloys. *Eng. Fail. Anal.* **2024**, *165*, 108828. [[CrossRef](#)]
13. Fan, W.; Yang, X.; Chu, Q.; Li, W. An efficient synergistic double-sided friction stir spot welding method: A case study on process optimization, interfacial characteristics and mechanical properties of 2198-T8 aluminum-lithium alloy joints. *J. Manuf. Process.* **2024**, *131*, 213–232. [[CrossRef](#)]
14. Tang, Y.; Li, W.; Zou, Y.; Wang, W.; Xu, Y.; Vairis, A.; Çam, G. Effects of tool rotation direction on microstructure and mechanical properties of 6061 aluminum alloy joints by the synergistically double-sided friction stir welding. *J. Manuf. Process.* **2024**, *126*, 109–123. [[CrossRef](#)]
15. Tier, M.D.; Rosendo, T.S.; Santos, J.F.D.; Huber, N.; Mazzaferro, J.A.; Mazzaferro, C.P.; Strohaecker, T.R. The influence of refill FSSW parameters on the microstructure and shear strength of 5042 aluminium welds. *J. Mater. Process. Technol.* **2013**, *213*, 997–1005. [[CrossRef](#)]
16. Cao, Y.; Zhang, C.C.; Xing, Y.F.; Wang, M. Pin plunging reinforced refill friction stir spot welding of Alclad 2219 to 7075 alloy. *J. Mater. Process. Technol.* **2020**, *284*, 116760. [[CrossRef](#)]
17. Han, B.; Huang, Y.; Lv, S.; Wan, L.; Feng, J.; Fu, G. AA7075 bit for repairing AA2219 keyhole by filling friction stir welding. *Mater. Des.* **2013**, *51*, 25–33. [[CrossRef](#)]
18. Sharma, A.; Khan, Z.A.; Siddiquee, A.N. Review of various methods of keyhole removal in friction stir welding sheets and pipes. *Mater. Today Proc.* **2022**, *62*, 404–409. [[CrossRef](#)]
19. Shen, Z.; Li, W.Y.; Ding, Y.; Hou, W.; Liu, X.C.; Guo, W.; Chen, H.Y.; Liu, X.; Yang, J.; Gerlich, A.P. Material flow during refill friction stir spot welded dissimilar Al alloys using a grooved tool. *J. Manuf. Process.* **2020**, *49*, 260–270. [[CrossRef](#)]
20. Li, Y.; Sun, G.; Zhang, Z.; Zhou, L.; Guo, N.; Meng, Q.; Dong, J.; Zhao, H. Texture evolution of refill friction stir spot welding in alclad 2A12-T42 aluminum alloy. *Mater. Charact.* **2023**, *205*, 113289. [[CrossRef](#)]
21. Shen, Z.; Ding, Y.; Gopkalo, O.; Diak, B.; Gerlich, A.P. Effects of tool design on the microstructure and mechanical properties of refill friction stir spot welding of dissimilar Al alloys. *J. Mater. Process. Technol.* **2018**, *252*, 751–759. [[CrossRef](#)]
22. Fritsche, S.; Draper, J.; Toumpis, A.; Galloway, A.; Amancio-Filho, S.T. Refill friction stir spot welding of AlSi<sub>10</sub>Mg alloy produced by laser powder bed fusion to wrought AA7075-T6 alloy. *Manuf. Lett.* **2022**, *34*, 78–81. [[CrossRef](#)]
23. de Castro, C.C.; Shen, J.; Plaine, A.H.; Suhuddin, U.F.H.; de Alcântara, N.G.; Santos, J.F.D.; Klusemann, B. Tool wear mechanisms and effects on refill friction stir spot welding of AA2198-T8 sheets. *J. Mater. Res. Technol.* **2022**, *20*, 857–866. [[CrossRef](#)]
24. Ferrari, V.R.; Coury, F.G.; Suhuddin, U.F.H.; Alcântara, N.G.; Santos, J.F.D.; Ohashi, R.; Fujimoto, M.; Koga, G.Y. Effects of semi-solid structure on interface formation of dissimilar aluminum to galvanized steel welds produced by load-controlled refill friction stir spot welding. *J. Manuf. Process.* **2022**, *84*, 298–315. [[CrossRef](#)]
25. Fu, B.; Shen, J.; Suhuddin, U.F.H.R.; Chen, T.; Santos, J.F.D.; Klusemann, B.; Rethmeier, M. Improved mechanical properties of cast Mg alloy welds via texture weakening by differential rotation refill friction stir spot welding. *Scripta Mater.* **2021**, *203*, 114113. [[CrossRef](#)]
26. Fu, B.; Shen, J.; Suhuddin, U.F.H.R.; Pereira, A.A.C.; Maawad, E.; dos Santos, J.F.; Klusemann, B.; Rethmeier, M. Revealing joining mechanism in refill friction stir spot welding of AZ31 magnesium alloy to galvanized DP600 steel. *Mater. Des.* **2021**, *209*, 109997. [[CrossRef](#)]
27. Yu, M.; Zhao, H.; Zhang, Z.; Zhou, L.; Song, X. Friction surfacing assisted refilled friction stir spot welding of AA6061 alloy and Q235 steel. *J. Manuf. Process.* **2022**, *77*, 1–12. [[CrossRef](#)]
28. Wang, S.; Wei, X.; Xu, J.; Hong, J.; Song, X.; Yu, C.; Chen, J.; Chen, X.; Lu, H. Strengthening and toughening mechanisms in refilled friction stir spot welding of AA2014 aluminum alloy reinforced by graphene nanosheets. *Mater. Des.* **2020**, *186*, 108212. [[CrossRef](#)]

**Disclaimer/Publisher’s Note:** The statements, opinions and data contained in all publications are solely those of the individual author(s) and contributor(s) and not of MDPI and/or the editor(s). MDPI and/or the editor(s) disclaim responsibility for any injury to people or property resulting from any ideas, methods, instructions or products referred to in the content.